Advances in River Sediment Research – Fukuoka et al. (eds)
© 2013 Taylor & Francis Group, London, ISBN 978-1-138-00062-9

Supercritical flow in sediment bypass tunnels

I. Albayrak, C. Auel & R.M. Boes
Laboratory of Hydraulics, Hydrology and Glaciology (VAW), ETH Zurich, Zürich, Switzerland

ABSTRACT: This paper deals with an experimental investigation of the mean and turbulence characteristics of supercritical quasi-uniform and gradually varied open-channel flows over a transitional rough bed. These conditions are typical for sediment bypass tunnels. The results show that the log-law holds well in the inner region across the channel. The roughness shifts the velocity profiles downward by an amount of ΔU^+. The velocity-dip phenomenon and strong secondary currents exist in the channel for narrow open-channel flow. These currents cause the Reynolds shear stress distributions to deviate from the linear distribution and an undulation on the transversal distribution of the bed shear stress, which matches with the bed abrasion pattern. The streamwise turbulence intensity profiles deviate from the semi-empirical universal function whereas the vertical turbulence intensity profiles fit well with it only at the centerline of the channel. A strong wall effect exists on the turbulence intensities in the outer region.

1 INTRODUCTION

Sediment bypass tunnels are an effective measure to decrease the reservoir sedimentation by routing the sediments into the dam tailwater during floods. However, due to supercritical open-channel flow condition and extensive sediment transport, most sediment bypass tunnels worldwide are affected by hydro-abrasion of the tunnel invert resulting in high annual maintenance costs (Vischer et al. 1997, Sumi et al. 2004). To mitigate the hydro-abrasion problem, a research project was initiated at the Laboratory of Hydraulics, Hydrology and Glaciology (VAW) of ETH Zurich. The main goal of the project is to establish general design criteria for optimal hydraulic conditions where sediment depositions in the tunnel are avoided and resulting abrasion damages are kept at a minimum. To achieve the goals, in this project, we investigate: (1) mean and turbulence characteristics of a supercritical turbulent open-channel flow at high Froude numbers (clear water experiments); (2) the sediment transport modes i.e. rolling, sliding, saltating, or suspension under different flow conditions; and (3) the relationship between the particle transport modes and rates, and the bed abrasion depth. This paper deals with the first part of the project by presenting a part of the results of the experimental investigation on the flow characteristics of quasi-uniform and gradually varied turbulent open-channel flows over transitionally rough boundary at high Froude numbers. The following literature review focusses only on this topic.

2 BACKGROUND

The flow characteristics in an open-channel are important and necessary to be clarified in order to solve many hydraulic engineering problems, particularly channel erosion and deposition problems. Over the past decades, various comprehensive researches have been carried out on mean and turbulence characteristics of fully developed open-channel flow over smooth and rough beds to advance in the understanding of the mechanics of turbulent flows and to quantify important flow parameters (Nikuradse 1933, Kline et al. 1967, McQuivey & Richardson 1969, Blinco & Partheniades 1971, Grass 1971). The boundary layer of open-channel flow can be divided into inner and outer regions. The logarithmic Prandtl-Karman type velocity distribution known as 'log-law' exists in the inner region and may extend to the outer region (von Kármán 1930, Prandtl 1932, Schlichting 1979, Nezu & Nakagawa 1993) and its formula universally follows:

$$U^+ = \frac{1}{\kappa}\ln(z^+) + A \quad (z^+ > 30) \tag{1}$$

where $U^+ = U/u_*$, U is the mean velocity, u_* is the friction velocity, $z^+ = zu_*/\upsilon$, z is the distance from the wall, υ is the kinematic viscosity, κ is the von Kármán constant and A is an integral constant. For transitionally and completely rough beds, the log-law includes the roughness shift ΔU^+ in Equation 1, or the length scale represented by

Nikuradse's equivalent sand roughness height k_s and follows as respectively:

$$U^+ = \frac{1}{\kappa}\ln(z^+) + A - \Delta U^+ \quad (2)$$

$$U^+ = \frac{1}{\kappa}\ln\left(\frac{z}{k_s}\right) + B \quad (3)$$

or

$$U^+ = \frac{1}{\kappa}\ln\left(\frac{z}{z_0}\right) \quad (4)$$

where z_0 is the zero-velocity level from the channel bed, B is an integral constant. For a completely rough bed $B = 8.5 \pm 15\%$ (Cardoso et al. 1989) or 8.47 ± 0.90 (Kironoto & Graf 1994) and for smooth and transitionally rough beds, B is the function of $k_s^+ = k_s\, u_*/\upsilon$, called 'roughness Reynolds number'. The boundary regimes are classified using k_s^+ and the relationships between z_0 and k_s (Nikuradse 1932, Schlichting 1979, Duan 2004) are given as:

$$k_s^+ < 5, \quad z_0 = 0.11\frac{\upsilon}{u_*} \text{ (smooth regime)} \quad (5)$$

$$5 < k_s^+ < 70, \quad z_0 = 0.11\frac{\upsilon}{u_*} + 0.033k_s, \text{ (transitional)} \quad (6)$$

$$k_s^+ > 70, \quad z_0 = 0.033k_s \text{ (rough regime)} \quad (7)$$

The universality of $\kappa = 0.41 \pm 5\%$ is verified by many investigations for steady fully developed closed- and open-channel flows over smooth, rough and even movable beds irrespective of Reynolds and Froude numbers (Coles 1956, Schlichting 1979, Cardoso et al. 1989, Tominaga & Nezu (1992), Nezu & Nakagawa 1993, Prinos & Zeris 1995, Kirkgoz & Ardiclioglu 1997).

In a long straight uniform river or open-channel section secondary currents of Prandtl's second kind driven by turbulence anisotropy exist and their strength and influence depends on the aspect ratio of the channel width b to water depth h. These large-scale streamwise vortical structures create zones of alternating up- and down-flows resulting in increased bed shear stresses in the down flow regions compared to neighboring upflow regions and redistribute Reynolds stress and turbulence intensities in relation to the bed shear stresses across the channel (Einstein & Li 1958, Nezu & Rodi 1985, Nezu & Nakagawa 1993, Rodrigues & Garcia 2008, Albayrak & Lemmin 2011). Thus, they contribute to sediment transport near the channel bed and change the channel bed form. Furthermore, in narrow open-channels with the aspect ratio < 5 the maximum velocity occurs just below the water surface due to the strong secondary currents, that is called 'velocity dip-phenomenon' (Rajaratnam & Muralidhar 1969, Nezu & Rodi 1985). In wide open-channels with aspect ratios $b/h > 5$, the secondary currents effect on the flow is still strong close to side-walls, but it weakens at the central zone and hence 2D flow is established (Nezu & Nakagawa 1993, Albayrak & Lemmin 2011).

From the available literature data and the conclusions drawn above it is evident that a lack of knowledge exists for mean and turbulence flow measurements at high Froude numbers for both uniform and non-uniform open-channel flows considering the effect of 2D and 3D flow structures. Therefore, in this study we investigate velocity and turbulence distributions in both steady quasi-uniform and gradually varied open-channel supercritical flows over a transitionally rough bed with the effect of aspect ratios. The goal of this experimental study is to measure the instantaneous and mean streamwise and vertical flow velocities across the channel and to obtain the spanwise bed shear stress, Reynolds shear stress and turbulence intensities distribution for typical flow conditions existing in sediment bypass tunnels at different flow depths. Additionally, as an example, first results from the bed abrasion experiments will be presented and compared with the present findings.

3 EXPERIMENTAL SETUP AND HYDRAULIC CONDITIONS

3.1 *Hydraulic model*

The experiments were conducted in a $b = 0.30$ m wide, 0.50 m high and 13.50 m long glass- and PVC-sided tilting laboratory channel (Fig. 1a). The channel bed was concrete lined and the bed slope was $S_b = 0.01$ for all experiments. The discharge Q was regulated with a magnetic flow-meter with an uncertainty of ± 0.5% and transferred from pressurized to supercritical free-surface flow using a jetbox (Schwalt & Hager 1992). The approach flow depth h_o at the jetbox was regulated with a gate. The flow depths h along the channel were measured with four Ultrasonic Distance Sensors (UDS) with an accuracy of ± 0.5 mm and verified by point gauge measurements with an accuracy of ± 0.2 mm. Velocity measurements were carried out at $x = 6.40$ m downstream of the jetbox. A typical velocity profile in an open channel flow is shown in Figure 1b.

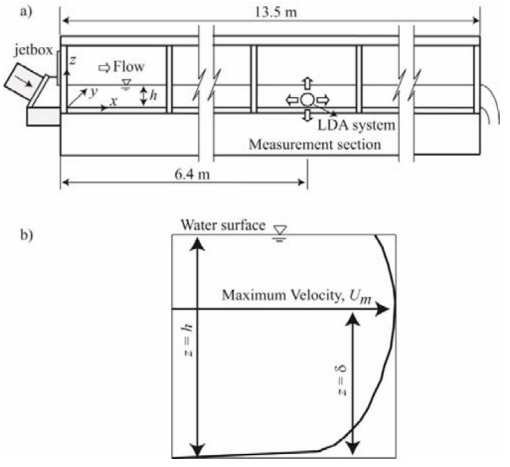

Figure 1. (a) Experimental setup and (b) typical velocity profile in an open channel flow.

3.2 *Test program*

Two of nine test runs are presented herein. These tests were conducted at the approach flow Froude numbers, $F_o = 2$ and 4 at the jet-box and coded as F2 and F4, respectively. The flow depth h_o was equal to 100 mm corresponding to the jet-box gate opening. The approach flow velocity U_o was obtained by the continuity equation $U_o = Q/(h_o b)$. The flow was fully developed and quasi-uniform for F2 and gradually varied for F4.

By using a 2D-LDA system FlowLite from Dantec Dynamics, data were collected for duration of 30 seconds at a frequency up to 1000 Hz at each of the 22 vertical profiles (Fig.1b) across the entire flume. Every vertical profile consisted to 24 measuring points resulting in a total of 528 measuring points per test run. Herein, five decisive vertical profiles at five traverse locations, y/b = 0.14, 0.33, 0.50, 0.66, 0.85, coded P1 to P5 are presented. Note that P3 is presenting the centerline.

The Froude F and the Reynolds numbers R, the water depth h, the mean cross-sectional velocity U and the maximum velocity U_{max} and the aspect ratio at x = 6.40 m downstream of the jetbox for the test runs are presented in Table 1.

3.3 *Bed roughness*

A detailed surface scan using a distance laser device was made at a 1.0 m long section in the measurement section, resulting in a scanned area of 300'000 mm^2 with 764 scanned measuring points. The mean value of the measured flume bed roughness heights is k = 0.2 mm.

Table 1. Hydraulic parameters for the experiments.

Test no.	F2	F4
h_o (m)	0.100	0.100
h (m)	0.106	0.117
b/h	2.8	2.6
U_o (m/s)	1.98	3.97
U (*) (m/s)	1.98	3.53
U_{max} (*) (m/s)	2.25	4.12
U_{*1} (m/s)	0.102	0.162
U_{*r} (m/s)	0.086	0.168
F_o	2	4
F	1.8	3.2
R (10^5)	4.7	8.9
k_s^+	34	34

(*) measured values at x = 6.40 m.

Furthermore, two methods were applied to determine the equivalent sand roughness height k_s. Firstly, k_{s1} = 0.20 mm is obtained using a backwater-curve calculation. Secondly, k_s was determined using the log-law formula (Equations 4 and 6). The average values of all vertical profiles are k_{s2} = 0.3 mm for F2 and 0.2 mm for F4. One can conclude that the real roughness height k and the calculated equivalent sand roughness heights k_{s1} and k_{s2} agree well.

3.4 *Friction velocity and bed shear stress*

To investigate the near-wall turbulence and to characterize sediment motion over a flume bed, it is important to evaluate the friction velocity u_* which is determined by applying two methods: (1) u_{*1} from the log-law (Equation 4) and (2) u_{*r} using the Reynolds shear stress distribution (Equation 8). According to Nezu and Nakagawa (1993) the Reynolds shear stress is the averaged product of the streamwise and vertical fluctuating velocities in a uniform open-channel flow and follows:

$$-\frac{\overline{u'w'}}{u_{*r}^2} = \left(1 - \frac{z}{h}\right) \tag{8}$$

The bed shear stress is obtained from the following:

$$\tau_b = \rho u_{*r}^2 \tag{9}$$

In the data analysis, the friction velocity obtained from the second method u_{*r} is used. In Table 1, U_{*1} and U_{*r} are the cross-sectional averaged values of the friction velocities, u_{*1} and u_{*r}, respectively. The values are in a reasonable agreement.

4 EXPERIMENTAL RESULTS AND DISCUSSIONS

4.1 *Mean velocity profiles related to secondary currents and dip-phenomena*

Figure 2 shows the mean streamwise velocity profiles P1 to P5 for F2 and F4 in inner variables together with the log-law fits developed from the measurements. In this figure, for each profile the zero axis where $U^+ = 0$ is shifted upwards by 5 and the relative position, δ of the maximum velocity, U_{max} is indicated by arrow. The von Kármán constant κ is 0.41 and remains the same as subcritical flow and the integral constant, A is taken as 5.29. In the wall region, the log-law (Equation 2) fits well with the experimental data not only in the centerline but also in the transversal locations. The aspect ratios for F2 and F4 are 2.8 and 2.6, respectively.

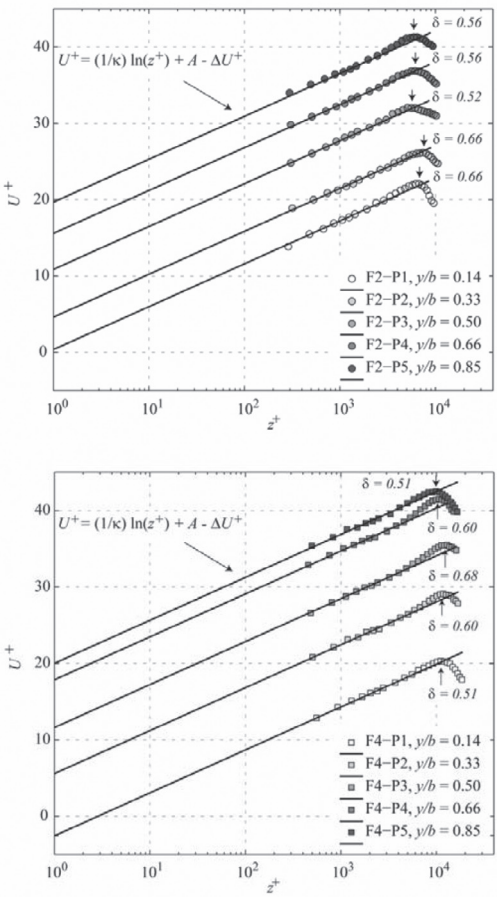

Figure 2. Mean streamwise velocity profiles in inner variables, together with the log-law fittings for F2 (a) and F4 (b).

According to Nezu and Nakagawa (1993) the transition from a 3D to 2D flow pattern occurs at $b/h > \alpha_c$, with $\alpha_c = 5$. Therefore, in the present case, the flow is three-dimensional. In Figures 2a & b the velocity dip phenomenon is clearly visible; maximum flow velocities do not develop close to the free surface, but at some distance below. The influence of the side wall frictions is evident, resulting in a 3D-flow pattern.

Particularly, the vertical positions of the maximum velocity in the transversal direction are not exactly symmetrical for F2 (compare F2-P1 and F2-P5 as an example) while it is symmetrical for F4. This asymmetry may be related to the effect of the different side walls i.e. glass wall at the right side and PVC wall at the left side or some other irregularity on the channel bed.

Figure 3 shows the velocity shift ΔU^+ as a function of roughness Reynolds number k_s^+ for F2 and F4 and compares them with the data from Schultz and Flack (2007) including Colebrook (1939), Nikuradse (1933) and Shockling et al. (2006). Note that κ, the integral constant, A and the relative roughness height in the present data are different than those found in the compared data. While the superpipe and Schultz and Flack data (2007) do not display the Colebrook-type monotonic behavior of the roughness function in the transitional regime, the present data clearly follow it and largely deviate from the Nikuradse-type behavior. At high k_s^+, the flow reaches the fully rough regime which agrees well with the compared data.

In the outer region of the boundary layer, the standard log-law should be adjusted by adding a wake function introduced by Coles (1956) instead of adjusting κ and A. Hence, the formula for the

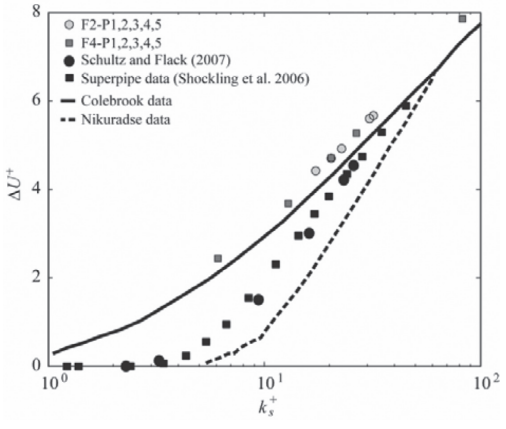

Figure 3. Velocity shift ΔU^+ of the present data F2 and F4 and literature data as function of k_s^+.

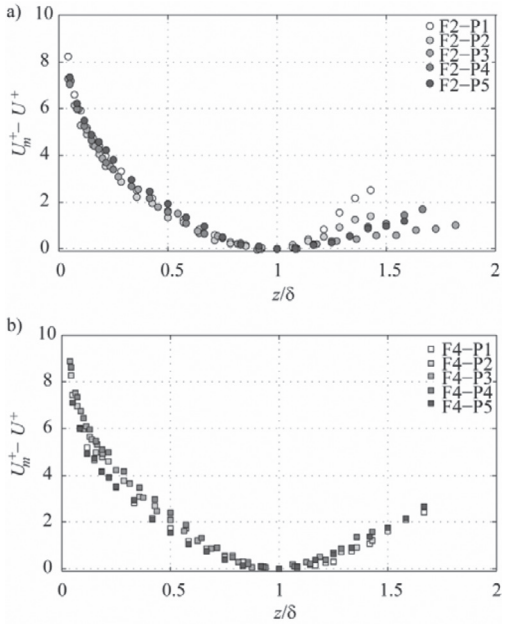

Figure 4. Mean velocity profiles in velocity defect form for F2 (a) and F4 (b).

velocity defect law including the Cole's wake function can be presented as:

$$U_m^+ - U^+ = -\frac{1}{\kappa}\ln\left(\frac{z}{\delta}\right) + \frac{2\Pi}{\kappa}\cos^2\left(\frac{\pi z}{2\delta}\right) \qquad (10)$$

in which, δ is the distance from the bed to the maximum velocity U_{max} (Fig. 1b) and $U_m^+ = U_{max}/u_*$.

Figures 4a & b show the outer-scaled mean velocity profiles in the velocity defect form for F2 and F4, respectively. No fitting of Equation 10 to the data is made since it is not our main focus in this study. The mean velocity profiles in the outer region are independent of k_s^+ and the transversal position, and collapse well for F2 while they are slightly scattered for F4 meaning that the surface roughness affect the velocity profiles only in the inner region. Close to the water surface, the velocity profiles for F2 deviate from each other showing an asymmetrical behavior due to different wall frictions whereas it is not so clear for F4.

4.2 *Reynolds shear stress*

Figure 5 show the Reynolds shear stress profiles normalized with the squared local friction velocity for F2 (a) and F4 (b) in outer scaling, together with the predictions from Equation 8. Most of the turbulence generation occurs on the edge of the inner region as seen in Figures 5a & b and the normalized Reynolds shear stress attain the maximum value between $z/h = 0.1$ and 0.2. On the one hand, the Reynolds shear stress distributions deviate from the expected linear trend (Equation 8) between the flume bed and the water surface, irrespective of Reynolds and Froude numbers, and the traverse positions. This deviation is associated with the secondary currents (3D flow). In the free surface region, the values of normalized Reynolds shear stress are negative for both F2 and F4. This is because dU/dz is also negative. On the other hand, the profiles approximately follow the linear trend when scaled with δ_m which is the average of the vertical positions δ of the maximum velocities (see $\delta_m/h = 1$ in Fig. 5). The data collapse well for F2 while they deviate slightly for F4 being high at the centerline and low at the side wall due

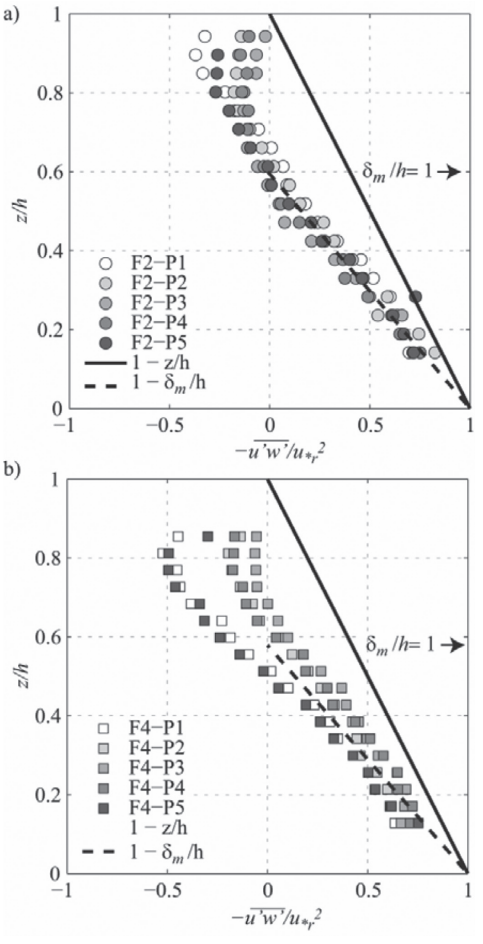

Figure 5. Normalized Reynolds shear stress profiles for F2 (a) and F4 (b).

to the much pronounced secondary current effect. Furthermore, the Reynolds shear stress distribution is rather concave than convex at the side walls due to the up flows. For all profiles, the damping effect of the water surface i.e. surface waviness on the Reynolds shear in the outer region is evident.

4.3 *Turbulence intensities*

The turbulence intensities in the streamwise and vertical direction, u_{rms} and w_{rms} denote root-mean-square values of the fluctuating component of the velocities, u' and w', respectively.

Figure 6 show the distribution of the streamwise turbulence intensity normalized by the local friction velocity u_{rms}/u_{*r} versus the relative water depth, z/h for F2 and F4 together with the universal function proposed by Nezu and Nakagawa (1993). The proposed function is:

$$u_{rms}/u_{*r} = 2.3e^{(-z/h)} \tag{11}$$

The agreement between the present data and Equation 11 are reasonable up to around $z/h = 0.5$, but still the measured streamwise turbulence intensity is slightly lower due to the roughness effect. A better fit can be obtained by adjusting the constants in the function.

The most striking feature seen in Figure 6 is that the maximum streamwise turbulence intensity occurs very close to the bed and then decreases gradually with z/h which agrees well with the previous open channel data and the Equation 11. However, above $z/h = 0.6$ for F2 and 0.5 for F4, the streamwise turbulence intensity strongly deviate from Equation 11 and increases due to corner vortices at the side walls.

Figure 7 shows the relative vertical turbulence intensity profiles w_{rms}/u_{*r} at five transversal

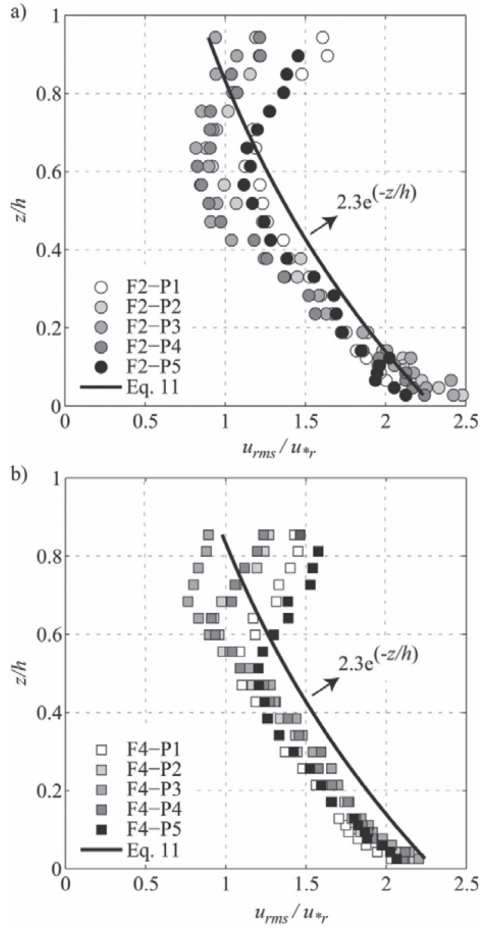

Figure 6. Relative streamwise turbulence intensity profiles for F2 (a) and F4 (b).

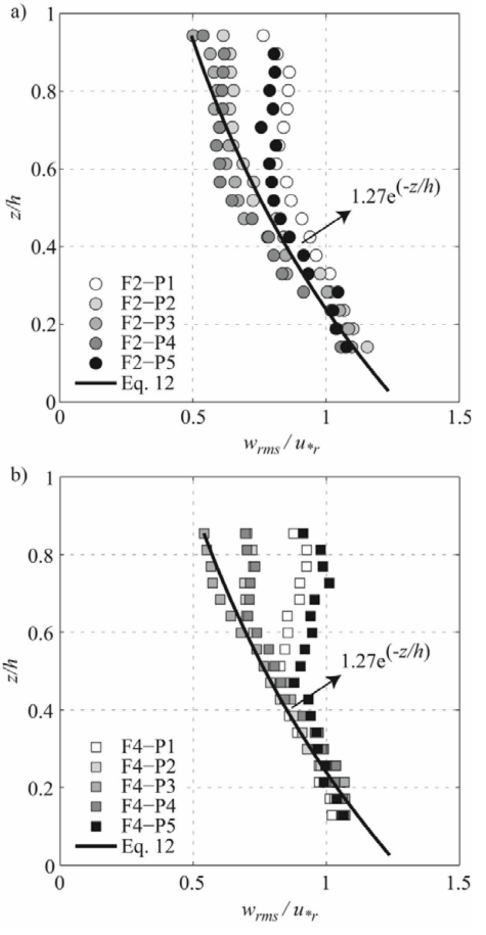

Figure 7. Relative vertical turbulence intensity profiles for F2 (a) and F4 (b).

positions for F2 (a) and F4 (b) together with the universal function for the vertical turbulence intensity distribution proposed by Nezu and Nakagawa (1993). The proposed function is:

$$w_{rms}/u_{*r} = 1.27e^{(-z/h)} \quad (12)$$

Contrary to the streamwise turbulence intensities, the relative vertical turbulence intensity profiles fit well with Equation 12 for both tests at the centerline over the whole water depth suggesting a non-clear influence of the aspect ratio and secondary currents, which agree well with the data in the literature (Nezu 1977). However, similar to the streamwise turbulence intensity, the profiles at the transversal positions of y/h = 0.14, 0.33, 0.66 and 0.85 begin to deviate from Equation 12 around $z/h = 0.6$ for F2 and $z/h = 0.5$ for F4 up to the water surface caused by strong vertical velocities due to strong corner vortices. Damping of water surface on the turbulence intensities similar to Reynolds shear stress are clear in Figures 6 & 7.

5 PRACTICAL APPLICATION OF THE FINDINGS

As described in the introduction, the bed abrasion due to high bed load transport in sediment bypass tunnels is a common problem. In order to mitigate this problem, the mean and instantaneous flow patterns, flow turbulence characteristics and importantly bed shear stress distribution across the channel have to be well clarified and quantified in a first step. Especially, the bed shear stress is the most influencing and governing parameter on the bed load transport calculations, sediment motions i.e. sliding, rolling and saltation, and the resulting bed abrasion pattern. Therefore, as an example of a practical engineering application of the present finding, the normalized bed shear distributions across the channel and the bed abrasion patterns obtained from the bed abrasion experiments (the third part of this research project, see introduction) are presented in Figure 8 for both test runs. The bed abrasion experiments were carried out with a mean grain size of 11 mm and 800 g/s sediment supply rate for F_o = 2 and 4 with a duration of 1.5 hours. In these experiments, the channel bed was covered with a weak mortar with the following parameters:

- Sand/cement ratio: 15:1
- Water/cement ratio: 0.6
- 1 mm grain size uniform sand
- Mean compression strength: 4.0 MPa
- Mean flexural tension: 0.6 MPa

Firstly, the bed abrasion pattern matches well with the bed shear stress distribution across the channel (Figures 8a & b). Close to the channel walls, the bed shear stress is about 20% higher than the cross-sectional averaged bed shear stress while it is approximately equal to the averaged bed shear stress at the center of the channel. The higher the bed shear stress, the higher the bed abrasion. The corner vortices at the channel bed which are different from the surface corner vortices cause even higher sediment transport from the bed and create two eroded channels at the side walls (Figures 8a & b). Secondly, the effect of the Froude number is obvious as the bed shear stress is almost 60% higher for F4 than for F2. Hence, the bed abrasion is much higher for F4.

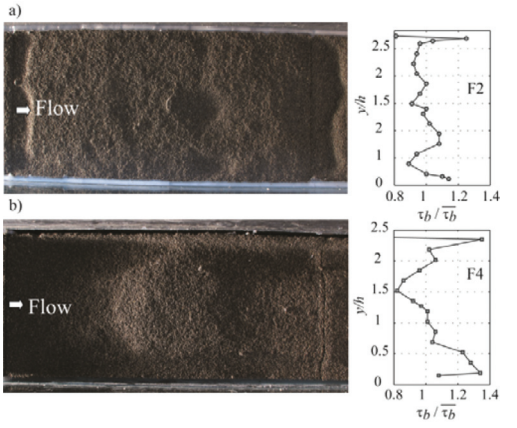

Figure 8. Bed abrasion patterns (Pletscher 2013) and corresponding bed shear stress distributions across the channel for F2 (a) and F4 (b).

6 CONCLUSIONS

Extensive and systematic experimental 2D-LDA velocity measurements were conducted in supercritical steady quasi-uniform and gradually varied open channel flows over a transitionally rough-bed. Previous studies documented the flow structures in a range of Froude numbers, aspect ratios and bed roughness. In this study, the measurements were made to cover even high Froude numbers up to F = 4, which is typical for some sediment bypass tunnels and has not been much studied yet (Auel and Boes 2011, 2012).

Streamwise velocity profiles were analyzed at five different transversal positions for the Froude numbers of 2 and 4. The results show that the log law still holds in the inner region ($y/h \leq 0.2$) across the channel even at high Froude numbers and gradually varied open-channel flow. The flow regime is transitionally rough and an increasing

roughness Reynolds number causes an increase in the downward shift in the overlap region of the velocity profiles. The roughness function follows rather the Colebrook-type monotonic behavior than the Nikuradse-type behavior.

The velocity dip phenomenon, i.e. the downward shift of the maximum velocity from the water surface, occurred in both experiments as expected for the aspect ratios smaller than 4 to 5. Maximum velocities were observed at relative flow depths of around $z/h \approx 0.6$ indicating that the outer flow region is affected by secondary currents. Although the velocity profiles collapse well in the outer region, they still need a wake correction.

As seen in the mean velocity profiles, secondary currents evidently change the distribution of the Reynolds shear stress, the turbulence intensities in the water column and across the channel. Hence, the undulation of the bed shear stress in the spanwise direction is directly associated with the existence of the secondary currents with strong bottom vortices at the side walls. This spanwise variation of the bed shear stress influences sediment transport and contribute to the formation of bed forms as observed in the bed abrasion experiments. Therefore, optimization of the hydraulic conditions in a bypass tunnel may help to mitigate bed abrasion.

To summarize, our results yield an important step towards the understanding of the mean and turbulence characteristics of a supercritical open channel flow over a transitionally rough bed and the interaction between the flow, sediment transport and bed abrasion. The follow-up study will focus on: (1) the flow characteristics of a wide open channel in a range of Froude numbers from 2 up to 8, (2) sediment transport modes of different size of particles and (3) their abrasion potential on the different bed materials and their interrelations.

ACKNOWLEDMENTS

The authors would like to thank *swisselectric research* and the Swiss Federal Office of Energy for their financial support.

REFERENCES

Albayrak, I. & Lemmin, U. 2011. Secondary currents and corresponding surface velocity patterns in a turbulent open-channel flow over a rough bed. *Journal of Hydraulic Engineering* 137(11): 1318–1334.

Auel, C. & Boes, R.M. 2011. Sediment bypass tunnel design—review and outlook. *Proc. 79th ICOLD Annual Meeting*, Lucerne, Switzerland, 403–412.

Auel, C. & Boes, R.M. 2012. Sustainable reservoir management using sediment bypass tunnels. *Proc. 24th ICOLD Congress*, Kyoto, Japan, 224–241.

Blinco, P.H. & Partheniades, E. 1971. Turbulence characteristics in free surface flows over smooth and rough boundaries. *Journal of Hydraulic Research* 9(1): 43–71.

Cardoso, A.H., Graf, W.H. & Gust, G. 1989. Uniform flow in a smooth open channel. *Journal of Hydraulic Research* 27(5): 603–616.

Coles, D. 1956. The law of the wake in turbulent boundary layer. *Journal of Fluid Mechanics* 1: 191–226.

Colebrook, C.F. 1939. Turbulent flow in pipes, with particular reference to the transitional region between smooth and rough wall laws. *Journals Institution of Civil Engineers* 11: 133–156.

Duan, J.G. 2004. Simulation of flow and mass dispersion in meandering channels. *Journal of Hydraulic Engineering* 130(10): 964–976.

Einstein H.A. & Li H. 1958. Secondary currents in straight channels. *Transactions—American Geophysical Union* 39(6): 1085–1088.

Grass, A.J. 1971. Structural features of turbulent flow over smooth and rough boundaries. *Journal of Fluid Mechanics* 50(2): 233–255.

Kirkgoz, M.S. & Ardiclioglu, M. 1997. Velocity profiles of developing and developed open channel flow. *Journal of Hydraulic. Engineering* 123(12): 1099–1105.

Kironoto, B.A. & Graf, W.H. 1994. Turbulence characteristics in rough uniform open-channel flow. *Proc. of the ICE—Water Maritime and Energy* 106(12): 333–344.

Kline, S.J., Reynolds, W.C, Schraub, F.A. & Runstadler, P.W. 1967. The structure of turbulent boundary layers. *Journal of Fluid Mechanics* 30(4): 741–773.

McQuivey, R.S. & Richardson, E.V. 1969. Some turbulence measurements in open-channel flow. *Journal of the Hydraulics Division* 95(HY1): 209–223.

Nezu, I. 1977. Turbulent structure in open-channel flows, *Ph.D thesis*, Kyoto Univ., Japan.

Nezu, I. & Nakagawa, H. 1993. Turbulence in open-channel flows. *IAHR Monograph*, Balkema, Rotterdam, NL.

Nezu, I. & Rodi, W. 1985. Experimental study on secondary currents in open channel flow. Proc., *21st IAHR Congress*, Vol. 2, Delft, Netherlands.

Nikuradse, J. 1933. Strömungsgesetze in rauhen Rohren. *Forschungsheft* 361, VDI-Verlag GmbH, Berlin, Germany (in German).

Nikuradse, J. 1932. Gesetzmäßigkeiten der turbulenten Strömung in glatten Rohren. *Forschungsheft* 356, VDI-Verlag GmbH, Berlin, Germany (in German).

Pletscher, B. 2013. Modellierung der Hydroabrasion. *Master thesis*, VAW, ETH Zurich, Switzerland (in German, unpublished).

Prandtl, L. 1932. Zur turbulenten Strömung in Rohren und längs Platten. *Ergebnisse der Aerodynamischen Versuchsanstalt zu Göttingen* 4, Oldenbourg, München, Germany, 18–29 (in German).

Rajaratnam, N. & Muralidhar, D. 1969. Boundary shear distribution in rectangular open channels. *La Houille Blanche*, Grenoble, France 24(6): 603–609.

Rodríguez, J.F. & García, M. 2008. Laboratory measurements of 3-D flow patterns and turbulence in straight open channel with rough bed. *Journal of Hydraulic Research* 46(4): 454–465.

Prinos, P. & Zeris, A. 1995. Uniform flow in open channels with steep slopes. *Journal of Hydraulic Research* 33(5): 705–719.

Schlichting, H. 1979. *Boundary layer theory. 7th ed. Springer*, Berlin, Germany.

Schultz, M.P. & Flack, K.A. 2007. The Rough-Wall Turbulent Boundary Layer from the Hydraulically Smooth to the Fully Rough Regime. *Journal of Fluid Mechanics* 580: 381–405.

Schwalt, M. & Hager, W.H. 1992. Die Strahlbox. *Schweizer Ingenieur und Architekt* 110(27/28): 547–549 (in German).

Shockling, M.A., Allen, J.J. & Smits, A.J. 2006. Roughness effects in turbulent pipe flow. *Journal of Fluid Mechanics* 564: 267–285.

Sumi, T., Okano, M. & Takata, Y. 2004. Reservoir sedimentation management with bypass tunnels in Japan. *Proc. 9th International Symposium on River Sedimentation*, Yichang, China.

Tominaga, A. & Nezu, I. 1992. Velocity profiles in steep open-channel flows. *Journal of Hydraulic Engineering* 118(1): 73–90.

Vischer D., Hager W.H., Casanova, C., Joos B., Lier P. & Martini, O. 1997. Bypass tunnels to prevent reservoir sedimentation. *Proc. 19th ICOLD Congress*, Florence, Italy.

von Kármán, T. 1930. Mechanische Ähnlichkeit und Turbulenz. *Nachrichten von der Gesellschaft der Wissenschaften zu Göttingen* 5: 58–76 (in German).